Current-free double-layer formation in inductively coupled plasma in a uniform magnetic field

S. Popescu,* Y. Ohtsu, and H. Fujita
Department of Electrical and Electronic Engineering, Saga University, Honjo-machi 1, Saga 840-8502, Japan
(Received 13 March 2006; published 23 June 2006)

The axial profiles of plasma parameters for low and moderate pressures, such as the plasma potential, electron temperature, and number density, have been evaluated in magnetized inductively coupled plasma. The experimental results revealed in both cases the existence of a genuine current-free double-layer structure, separating two plasma regions with different properties. Based on the experimental results, a physical scenario for the self-assembling of the double layer is proposed. Also, the axial profile of the electron number density downstream is analyzed, emphasizing the role of neutral metastable ionization, and a simple analytical model is developed to fit the experimental data. The model allows the estimation of neutral metastable number density downstream and the recombination rate coefficient.

DOI: 10.1103/PhysRevE.73.066405 PACS number(s): 52.40.Kh, 52.50.Qt, 52.25.Xz, 52.70.−m

I. INTRODUCTION

Plasma potential formations have aroused a strong interest ever since their first experimental characterization by Langmuir [1]. After emphasizing their importance in space plasma by Alfvén [2], electric double layers (DL's) have been extensively studied [3]. In the last two decades the number of works on this topic has continuously increased, no less than five international symposiums dedicated to DL's being organized during this period [4]. Moreover, their utility for space and technological applications has been continuously investigated.

The spontaneous appearance of "current-free DL's" during plasma expansion in a diverging magnetic field, in a helicon discharge, has been recently reported [5]. These "DL's" can form at rather low pressures (i.e., only below 1 mTorr) and represent a source of energy for the positive ions traversing them [5]. Although in the last two years a considerable number of papers have been published on this topic [6], Chen lately showed that these kinds of localized potential formations, emerging during plasma expansion in diverging magnetic fields, are in fact single layers, predictable from classical sheath theory [7].

The aim of this paper is to present experimental data on the appearance of genuine DL's in a magnetically enhanced inductively coupled plasma at low (i.e., less than 1 mTorr), but also at moderate, pressures (i.e., greater than 1 mTorr) and, on these bases, to formulate the physical scenario responsible for the appearance of DL's in radio-frequency (rf) discharges (i.e., the succession of physical processes underlying their emergence). This is an important task, because the understanding of the physical basis of the appearance of DL's is an essential step for formulating a realistic analytical model. Moreover, to explain the spatial evolution of the plasma number density downstream, the role of neutral metastable ionization is discussed and a simple analytical model for describing the density profile is formulated.

II. EXPERIMENTAL SETUP

The experiments were performed on a horizontal, magnetically enhanced inductively coupled plasma device, illustrated in Fig. 1. A three-turn, water-cooled, copper helical antenna (marked *A* in Fig. 1) surrounds a 4-cm-inner-diameter and 20-cm-long glass tube (labeled *T* in Fig. 1). The rf power applied to this coil, through a matching circuit, induces an electric field in the gas inside the glass tube, which partially ionizes the gas atoms and produces the discharge. The glass tube (i.e., the source chamber) is mounted coaxially at one end of a stainless-steel cylindrical vessel, 16 cm inner diameter and 116 cm long (i.e., the main chamber).

To increase the plasma density and reduce the wall bombardment the whole system was surrounded by seven magnetic coils (inner diameter 25 cm and outer diameter 53 cm), which produce an axial, static magnetic field $\mathbf{B}=B\hat{z}$, where $\hat{z}$ is the unit vector of the axial direction (i.e., parallel with the symmetry axis of the whole device). In order to decrease the number of variables and to investigate only the role of elementary and collective processes taking place in plasma for the appearance of potential structures of DL type, the magnetic coils were disposed in such a way that the magnetic field on the system's axis was uniform. The measured magnetic induction along the axis was $B=215\pm5$ G.

For controlling the processes inside the plasma, an Al disk collector (marked *C* in Fig. 1), 6 cm in diameter, was in-

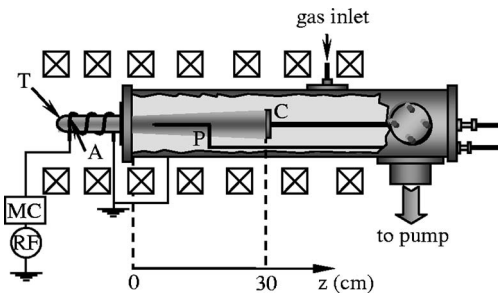

FIG. 1. Experimental setup. *A*: helical antenna. *T*: glass tube. *C*: collector. *P*: plane Langmuir probe. rf: radio-frequency power supply. MC: matching circuit.

*Permanent address: Department of Plasma Physics, "Al I Cuza" University, 700506 Iasi, Romania. Electronic address: seba@ep.ee.saga-u.ac.jp; seba@uaic.ro

serted into the main chamber, through its end plate, facing the plasma source. The lateral and rear parts of the collector were electrically insulated. The symmetry axis of the collector is along the axial direction $0z$ of the discharge tube and its position was fixed at $z=30$ cm inside the main chamber. For fixing the ideas, the origin of the z axis was chosen at the interface of the glass tube with the metallic one. The positive sense of this axis is towards the main chamber (i.e., downstream or $z>0$). Consequently, $z<0$ in the source chamber (i.e., upstream).

The plasma properties were measured with an rf-compensated Langmuir plane probe (marked P in Fig. 1)—i.e., a tungsten wire of 1 mm in diameter—laterally insulated, such that only its plane end faced the plasma source, along the axial direction. During the experiments the probe was axially moved between $z=-10$ cm and $z=+8$ cm. Because the probing range is relatively far from the end plate of the main chamber (over 1 m) and also for minimizing the plasma perturbation, the probe shaft was lying on the bottom of the metallic tube. In order to have the probe tip on the z axis, the probe was constructed with a dogleg, as can be seen from Fig. 1.

III. EXPERIMENTAL RESULTS

The experimental measurements were carried out using Ar as working gas, at moderate ($p>1$ mTorr) and low pressures ($p<1$ mTorr). The pressure-specific values at which the experiments were performed are 2.0 mTorr and 0.5 mTorr, respectively, one for each pressure range. The system obtained by joining the two chambers was vacuumed at the base pressure of 2×10^{-6} Torr, and the pressure was measured with an ionization vacuum gauge control. The rf input power was 200 W, with less than 0.5% reflection, at the working frequency of 13.56 MHz.

Throughout the experiments the collector was electrically floating (unless specifically stated otherwise) and all the plasma parameters were measured only in the axial direction. More exactly, all the probe measurements started from the center of the source chamber ($z=-10$ cm) and were carried out axially, in a single run, in the sense of $\hat{z}$. The time-averaged plasma (or space) potential was evaluated from the maximum of dI_e/dV, after smoothing the data to eliminate the digital noise [8]. Here I_e is the electron current (i.e., the current measured by the probe, after the subtraction of the ion component) and V is the probe potential with respect to the ground. In all cases the dI_e/dV curves exhibited a net maximum.

The visual appearance of the plasma was that of an axially confined luminous column, with the same diameter as the source chamber and extended between the source and collector. However, going downstream, the plasma column was slowly diverging, attaining the same diameter as the collector, in its proximity.

A. Low pressure ($p=0.5$ mTorr)

The spatial profile of the plasma potential V_s in the domain of interest is illustrated in Fig. 2(a). It can be seen

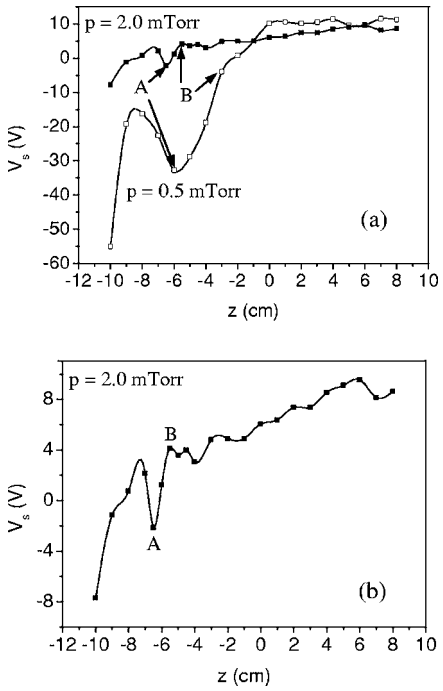

FIG. 2. Axial profile of the plasma potential V_s when the collector is electrically floating at $p=0.5$ mTorr (□) and $p=2.0$ mTorr (■); (b) is a detail of the same curve represented in (a).

that, starting from the center of the source chamber, after a relatively abrupt increase ($dV_s/dz=36$ V/cm), the space potential starts to decrease, with a smaller rate ($dV_s/dz=-8$ V/cm), attaining a minimum $V_s=-33$ V at $z=-6$ cm [point marked A in Fig. 2(a)]. Beyond this region, the plasma potential increases with a higher rate ($dV_s/dz=10$ V/cm), reaching after that a saturation value at about $V_s=+11.5$ V.

Upstream, the electron temperature T_e [Fig. 3(a)] displays a profile similar to that of the plasma potential; namely, after an abrupt growth in the center of the source chamber ($dT_e/dz=8.8$ eV/cm), it decreases to a minimum ($T_e=13$ eV) located at $z=-6$ cm [point A in Fig. 3(a)], to increase after that to a local maximum ($T_e=17.7$ eV) at about $z=-2$ cm. Downstream, the electron temperature decreases with a rate of about $dT_e/dz=2.2$ eV/cm to attain a value of 10 eV at $z=7$ cm. The electron temperature was evaluated in this case using the relation

$$V_s = V_f + \alpha T_{e,eV}, \tag{1}$$

where V_f is the floating potential and α a coefficient, depending on the ion to electron mass ratio. The value of this constant for Ar was taken $\alpha=5.4$ [8,9] to also include the plasma fluctuations. We used this approach because upstream the linearity domain of the semilogarithmic plot $\ln I_e(V)$ was ensured for less than one order of magnitude of I_e variation. The axial profile of the electron temperature evaluated from the slope of the semilogarithmic plot in this case was the same as that displayed in Fig. 3, but shifted towards higher, hence more unrealistic, values for the kinetic temperature of electrons.

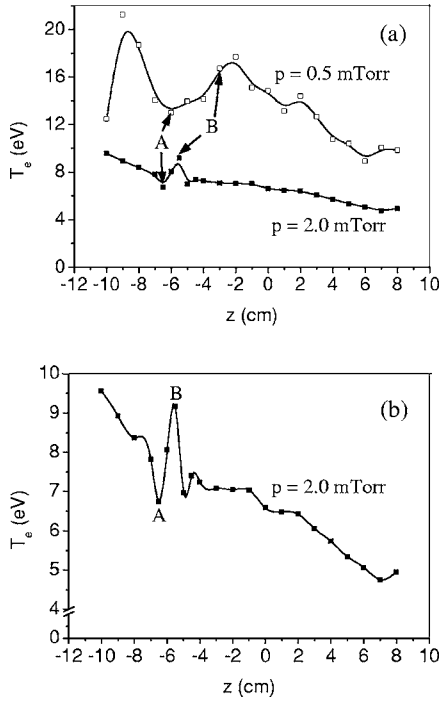

FIG. 3. Axial representation of the electron temperature T_e at $p=0.5$ mTorr (□) and $p=2.0$ mTorr (■); (b) is a detail of the same curve represented in (a).

The axial dependence of plasma number density is plotted in Fig. 4. It shows that, after a spatial domain (situated close to the middle of the plasma source—i.e., between $z=-10$ cm and $z=-8$ cm) in which the density is almost constant ($n=6.4\times10^8$ cm^{-3}), going downstream the density is slowly and monotonically increasing, at $z=8$ cm its value being $n=1.1\times10^{10}$ cm^{-3}.

B. Moderate pressure ($p=2.0$ mTorr)

The axial profile of the plasma potential in the probing domain is plotted in Fig. 2, it being closer to the ground potential than in the low-pressure case. This profile also reveals that, after a relatively steep increase ($dV_s/dz=7.7$ V/cm) inside the source chamber, the space potential still grows downstream, but with a much slower rate ($dV_s/dz=0.5$ V/cm). These two distinct regions are connected by a potential dip of $\Delta V_s=6.25$ V, located at $z=-6.5$ cm [marked A in Fig. 2(b)].

The electron temperature profile, represented in Fig. 3, displays a marked slope ($dT_e/dz=0.6$ eV/cm) inside the source chamber, while downstream the decrease is slower ($dT_e/dz=0.3$ eV/cm). Between these regions the electron temperature has a peak of $\Delta T_e=2.4$ eV at $z=-5.5$ cm [marked B in Fig. 3(b)]. At this pressure, due to the good linearity of the semilogarithmic representation of I_e as a function of probe potential, the electron temperature was evaluated from the slope of this plot. However, the use of Eq. (1) for evaluating the electron temperature in this case gives a profile similar with that represented in Fig. 3(b), with very small differences in the temperature values for each axial probed position.

The profile of the electron number density is shown in Fig. 4. It shows that going downstream, the electron number density increases and saturates at about 1.7×10^{10} cm^{-3}, starting from $z=6$ cm. In both pressure ranges the axial profiles of the electron number density show that going downstream n_e increases.

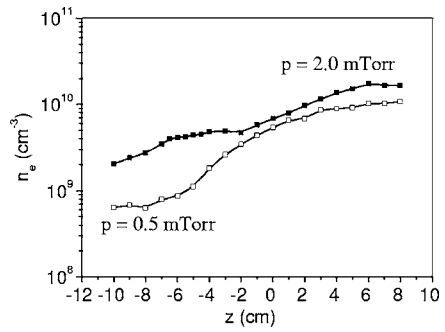

FIG. 4. Axial variation of the electron number density n_e at $p=0.5$ mTorr (□) and $p=2.0$ mTorr (■).

IV. DISCUSSION

Examining comparatively the experimental results obtained in both pressure ranges, some immediate conclusions can be drawn. First, in both cases the plasma potential is negative inside the source chamber and positive downstream. This is due to the fact that the glass tube is electrically floating, while the metallic wall of the main chamber is grounded. Under these circumstances, immediately after the ignition of the discharge, the glass wall of the source chamber is charging negatively. This process is sustained by the fact that the floating potential measured by the Langmuir probe inside the glass tube is well below 0 V: between −140 V and −70 V at $p=0.5$ mTorr and between −60 V and −20 V at $p=2$ mTorr. Second, for both pressure ranges the axial dependences of the physical quantities of interest have the same profile, although their variations in the source chamber at low pressure are bigger than those at intermediate pressure.

Increasing the gas pressure it can be seen that the well appearing in the plasma potential profile narrows (Fig. 2) and it is present at the same axial coordinate ($z\cong-6$ cm). The same behavior is also valid for the electron temperature (Fig. 3). Moreover, as the pressure increases four times, the height of the above potential well decreases approximately with the same ratio. At both pressures, going downstream, the electron number density monotonically increases (Fig. 4), it being one order of magnitude higher at $z=8$ cm than in the center of the source chamber. Due to this behavior of the electron number density downstream, we preferred to name the downstream region the "main chamber" and not the "diffusion chamber," as it is usually called [5].

In order to simplify the discussion and to sketch the physical scenario underlying the obtained experimental results, in the following we will make the analysis separately for each zone—i.e., upstream and downstream.

A. Upstream

At both pressures, it can be seen that, starting from the center of the source chamber, the plasma potential increases first with a relatively big slope, to reach a positive, relative constant value of about 10 V downstream. The z dependences of the plasma potential for both pressure ranges have similar profiles. They present a local minimum which separates two plasmas with different properties. Starting from this local minimum the profile of the plasma potential is that of an electric DL.

In the low-pressure case, going downstream from the center of the source chamber, the electrons are accelerated by a strong electric field [of about 36 V/cm, as can be seen from Fig. 2(a)], gaining enough energy to excite the neutrals. The decrease of electron kinetic temperature, beginning with $z=-9$ cm, indicates that they lose some of their energy by exciting the neutrals. As a result, at about $z=-6$ cm, where the electron temperature reaches its local minimum, the electrons that lose their kinetic energy by exciting the neutrals will accumulate and form a net negative space charge there. This assertion is sustained by the informational content of Fig. 2(a), the space potential presenting a local minimum in the same location. The electrons that have not excited the neutrals are further accelerated downstream by a local electric field of about 10 V/cm [Fig. 2(a)]. At $z=-3$ cm, the kinetic energy of electrons surpasses the ionization energy of the neutrals in the fundamental state [Fig. 3(a)]. The result is the appearance of a net positive space charge located there [point B in Fig. 2(a), where the space potential as a function of axial distance changes from a convex to a concave function—evidence of a net positive space charge there]. The electrons ionizing the neutrals, as well as those resulting after ionization, are accelerated downstream.

For the intermediate-pressure case, the experimental results show that the plasma electrons produced inside the source chamber are accelerated towards the main chamber [Fig. 2(b)] by a relatively strong axial electric field ($E_z=7.7$ V/cm). In this way, on a short distance (between $z=-11$ cm and $z=-9$ cm), the electrons could, in principle, gain sufficient energy for ionizing the neutrals, but in the same region the electron temperature begins to decrease [Fig. 3(b)], due to inelastic collisions with the neutrals. This means that the sudden decrease of the space potential and of the electron temperature at $z=-6.5$ cm [point A in Figs. 2(b) and 3(b)] is the result of neutral excitation by electron collisions. Consequently, the electrons exciting the neutrals gather there and form a net negative space charge, explaining in this way the existence of the two local minima (for V_s and T_e) at $z=-6.5$ cm. Following the same succession of processes as above, the electrons that have not excited the neutrals are further accelerated by the electric field and, after traveling about 1 cm downstream from the net negative space charge, are rich enough in kinetic energy to ionize the neutrals. Thus, this physical scenario explains the sudden increase of the electron temperature at $z=-5.5$ cm, as well as that of the plasma potential in the same place [point B in Figs. 2(b) and 3(b)]. The electrons that ionize the neutrals and those resulting from this process are accelerated downstream by the electric field.

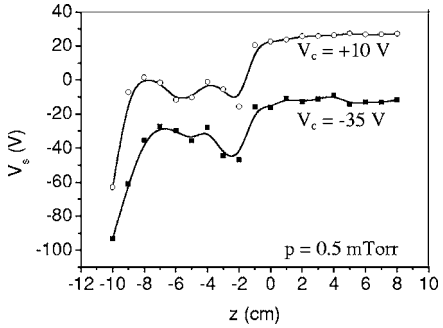

FIG. 5. Axial profile of the plasma potential V_s when the gas pressure is $p=0.5$ mTorr and the collector is biased: $V_c=+10$ V (○) and $V_c=-35$ V (■).

In both cases, the electrostatic forces of attraction between these two adjacent, opposite space charges, created inside of the source chamber, acting as long-range correlations, "bind" them together. The result is the self-assembling of an electric DL, which will accelerate electrons downstream [10]. In the low-pressure case, the potential drop on the DL is $\Delta V_{DL}=29$ V and its thickness $\Delta z_{DL}=3$ cm $\cong 136\lambda_{De}$, where λ_{De} is the Debye length for electrons. Taking into account that the electron temperature downstream is $T_{e,eV}=10$ eV, the strength of this DL is $\eta_{DL}\equiv\Delta V_{DL}/T_{e,eV}\cong 3$. Moreover, the thermal barrier across the DL is $\Delta T_e=3.7$ eV. In the intermediate-pressure case, the potential drop on the DL is $\Delta V_{DL}=6.25$ V and its thickness $\Delta z_{DL}=1$ cm $\cong 77\lambda_{De}$. Also, the thermal barrier across the DL is, in this case, $\Delta T_e=2.4$ eV. Comparing the value of the potential drop on the DL with the electron temperature downstream, the strength of the DL can be obtained: $\eta_{DL}=\Delta V_{DL}/T_{e,eV}=1.25$. Analyzing these numerical results for both cases, it follows that at low pressures the DL is stronger and thicker than the DL appearing at intermediate pressures. Certainly, there will be a threshold pressure, not much higher than 2.0 mTorr, for which the ionization cross section for neutral ionization will not grow abruptly anymore at a certain location, to give birth to the positive net space charge needed for the DL self-assembling. So DL's can spontaneously appear only for pressures smaller than the above threshold value.

The appearance of DL's in the cases analyzed by us, in the absence of an externally imposed conduction current, the collector being floating ($V_{c,f}=-11.2$ V), gives them the quality of being current free. If the collector is not floating, but biased, the DL will be current driven. Figure 5 displays the plasma potential profiles obtained for two dc voltages applied to the collector ($V_c=-35$ V and $V_c=+10$ V, respectively). The curves represented in Figs. 2(a) and 5 have similar profiles, and the important feature they emphasize is the controlling role of the collector: by biasing it, the DL narrows and shifts towards $z=0$ cm. Of course, in the latter case the DL will not be current free anymore.

To analyze if the DL is planar [two dimensional (2D)] or bulging (3D), we will use the scaling of the DL potential drop with the parameter $j(\Delta z_{DL})^2$, where j is the current density across the DL, similar to that proposed in [11]:

$$\Delta V_{DL} = [\beta j (\Delta z_{DL})^2]^r, \quad (2)$$

where $\beta = \frac{9}{4\varepsilon_0}\sqrt{\frac{m}{2e}}$, m and e being the mass and electric charge of electron, respectively, and ε_0 the vacuum permittivity. In Eq. (2), the positive exponent r takes the value 2/3 for the plane DL and decreases as the DL curvature increases [11]. It is worthwhile to note here that in the case of planar DL's, Eq. (2) is nothing else than the relation found by Langmuir for DL's [1], which is just the Child-Langmuir law. Making use of Eq. (A5) from Appendix A for the current density, Eq. (2) yields the numerical value of the exponent of interest: $r = 0.30$ for $p = 0.5$ mTorr and $r = 0.19$ for $p = 2$ mTorr. The obtained estimations indicate that the DL's obtained in our experiments are not planar, but bulging. Moreover, as the pressure increases, the curvature of the DL increases.

B. Downstream

Going downstream, the electron number density increases in both pressure ranges (Fig. 4). This means that the ionization rate increases with z, although the electrons do not seem to have enough kinetic energy to ionize the ground-state neutrals (Fig. 3). This apparent contradiction can be eliminated by considering the neutral metastable ionization, as an additional source of electrons.

For the low-pressure case, starting with $z = 1$ cm, the plasma is unperturbed [Fig. 2(a)], its potential being constant ($V_s \cong 11.5$ V). Because the electron temperature decreases [Fig. 3(a)], it means that the electrons, accelerated inside the DL potential drop, are still losing kinetic energy in inelastic collisions. If at $z = -2$ cm their kinetic energy surpasses the ionization energy of the argon neutrals in the fundamental state ($W_i = 15.76$ eV), in the range -2 cm $< z < 3$ cm the electron energy is enough only to excite the ground-state neutrals (in $z = 3$ cm their energy being $W_{k,e} = 12.65$ eV, while the first excitation level, which is a metastable one, has the energy 11.55 eV) and to ionize the neutral metastables.

In the moderate-pressure case, starting with $z = -4$ cm the electron temperature also decreases [Fig. 3(b)]. Though it is not enough to ionize the neutrals, the electrons still have sufficient kinetic energy to ionize the neutral metastables. The metastables can be produced in this case only by the electrons from the high-energy tail of the distribution function. For this reason, we expect the metastable number density at moderate pressure to be lower than that in the low-pressure case. Another argument for sustaining this affirmation is offered by Fig. 4. In the low-pressure case the increase of the electron number density is more accentuated than at moderate pressures. Numerical simulations seem to endorse the above assertion, showing that the ratio of metastable to ground-state density increases with decreasing pressure [14].

Usually, the population of the excited levels decreases exponentially with energy, in accordance with the Boltzmann distribution law, so the most populated energy levels are those situated closest to the fundamental level. Due to this argument, in the following discussion we will take into account only the $3p^6 \rightarrow 3p^5 4s^1$ electronic transitions. This simplification is not too far from reality (i.e., excitation of neutrals on higher-energy levels, under the present experimental conditions, is much less frequent than that on the 4s level) and illustrates in a simple manner the phenomena taking place in downstream plasma. The fine structure of the energy level 4s consists of four sublevels, as is illustrated in Fig. 6. Some of the properties of the energy states depicted in Fig. 6 are given in Table I.

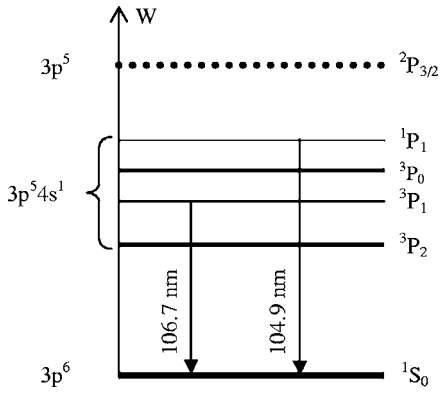

FIG. 6. Energy-level diagram for neutral Ar (not at scale), emphasizing the fine structure of the first excited level. The dotted line denotes the first ionization level, the base, thick one is the fundamental (ground-state) level, the thin lines are the resonant sublevels, and the rest of the lines, thicker than the resonant ones, are the metastable sublevels.

Because the resonant states $^3P_1$ and $^1P_1$ have lifetimes much shorter than the inverse of the electron collision frequency ($\nu_{en} \cong 5.23$ MHz at $p = 0.5$ mTorr and 14.86 MHz at $p = 2.0$ mTorr), the dynamics of the excited neutrals in these states is controlled by radiative decay and not by collisions. By the other hand, the neutrals in the metastable states $^3P_2$ and $^3P_0$, due to their long lifetimes compared with the inverse of the electron collision frequency, can be deexcited or ionized by collisions.

Taking into account that the threshold energy for excitation is below the ionization threshold, it seems logical to assume that the production rate of metastables is comparable with that of positive ions. In inductively coupled plasmas, the experimental measurements in Ar, in the pressure range of 4–50 mTorr, show that the spatial distribution of the metastable number density is quasiuniform, time independent, with a broad peak in the middle of the main chamber,

TABLE I. Properties of several energy levels of Ar.

Spectral term	Level type	Level energy (eV)	Lifetime (s)
$^2P_{3/2}$	Ionization	15.76	$\gg 1$
$^1P_1$	Resonant	11.83	2.5×10^{-9}[a]
$^3P_0$	Metastable	11.72	> 1.3[b]
$^3P_1$	Resonant	11.62	10.4×10^{-9}[a]
$^3P_2$	Metastable	11.55	> 1.3[b]
$^1S_0$	Fundamental	0	$\gg 1$

[a]Reference [12], p. 70.
[b]Reference [13].

and also that their number density is comparable with that of electrons [15]. Another argument sustaining the importance of the ionizing role of neutral metastables in sustaining rf discharges at low pressures is offered by the recent experiments developed in inductively coupled plasma modulated by short high-current pulsed discharges [16]: in gases without metastable excited states, like hydrogen, the plasma decays much faster than in gases with metastables, like argon.

So, assuming that the metastable number density is comparable with that of electrons and taking into account that at both pressures the electron kinetic energy downstream is enough to ionize the Ar metastables ($W_{k,e} > 4.21$ eV), the increase of the electron number density downstream can be explained by considering metastable ionization as an additional source of electrons.

Considering that the main processes which can modify the electron number density on the axis are diffusion and recombination, as well as ground-state neutral and metastable ionization, the balance equation for electrons reads

$$\frac{\partial n_e}{\partial t} - D_a \frac{\partial^2 n_e}{\partial z^2} = (k_1 n^* + k_2 n_n) n_e - k_3 n_i n_e^2, \tag{3}$$

where $D_a \equiv \frac{D_e \mu_i + D_i \mu_e}{\mu_e + \mu_i} \cong \frac{e\langle T_{e,eV}\rangle}{M \nu_{in}}$ is the ambipolar diffusion coefficient (which is the diffusion coefficient for the direction parallel with the magnetic field), $D_{e,i}$ and $\mu_{e,i}$ are electron and ion diffusivities and mobilities, respectively, M the ion mass, ν_{in} the ion-neutral collision frequency, and $\langle T_{e,eV}\rangle$ the mean electron temperature measured in eV. The significance of the rest of quantities appearing in Eq. (3) is the following: $n_{e,i,n}$ the electron, ion, and neutral number densities, respectively, n^* the metastable number density, $k_{1,2}$ the ionization rate coefficients from metastable and fundamental levels, respectively, and k_3 the rate coefficient for three-body recombination in the presence of an electron. We took into account this process for ensuring the concomitant conservation of momentum and energy for the recombinations taking place on the axis, the role of the second electron being just to absorb the excess reaction energy. Even if the electron loss by two-body recombination is very unlikely on the axis, its importance will increase near a solid surface (i.e., the chamber wall or the collector), which plays the role of the third particle. However, the probing domain is far from the collector, such that its role of "sink" for electrons is not felt in the range $-10\ \text{cm} \leqslant z \leqslant +8\ \text{cm}$. Mathematically, the two-body recombination rate is a quadratic term in n_e. The addition of this rate to the right-hand side of Eq. (3), which is a cubic polynomial in n_e, does not change the form of the solution, because a linear transform of variable brings back the polynomial to its canonical form (i.e., without the quadratic term) and the new solution is just the old one shifted with a constant.

Taking into account that downstream the electric field and electron temperature gradient are low, in a first approximation, we can consider the rate constants and the diffusion coefficient as being constant. Taking the metastable number density as being constant downstream (due to the fact that the electron mean free path is comparable with the characteristic length of the discharge gap) and, also, that the ion

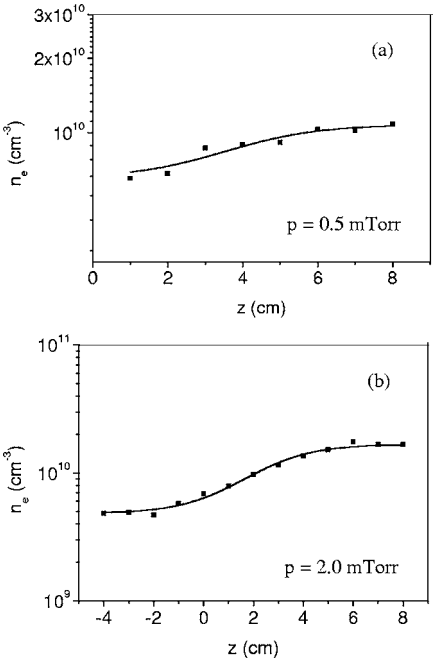

FIG. 7. Fitting of the experimental data for the electron number density downstream with the graphical representation of Eq. (5) at $p=0.5$ mTorr (a) and $p=2.0$ mTorr (b).

number density is equal to that of electrons, in the stationary state Eq. (3) becomes

$$\frac{\partial^2 n_e}{\partial z^2} = \xi n_e^3 - \psi n_e, \tag{4}$$

where $\xi = k_3/D_a$ and $\psi = (k_1 n^* + k_2 n_n)/D_a$ are constant coefficients. The solution of this equation is [Eq. (B5) from Appendix B]

$$n_e(z) = n_1 + n_0 \tanh\left[n_0 \sqrt{\frac{\xi}{2}} (z - z_0) \right], \tag{5}$$

$n_{0,1}$ and z_0 having the meaning given in Appendix B.

By fitting Eq. (5) to the experimental data (Fig. 7) we can estimate the neutral metastable concentration downstream, as well as the three-body recombination rate coefficient for Ar in our working conditions. The obtained results are shown in Table II. For obtaining these results we considered the ionization rate coefficient of neutral metastables k_1 to be two orders of magnitude larger than that of the ground state k_2 [17]. Of course, the obtained values for k_3 and n^* are overestimates, this approach being just a first order of approximation. First of all, we considered all the coefficients as being constant, neglecting their variation with axial distance and electron temperature, which we also considered constant and replaced by its mean value. Second, the metastable number density was assumed uniform. Of course, by taking into account other processes involving the neutral metastables, like metastable pooling, two-body and three-body quenching, and superelastic collisions involving metastables, as well as excitation of metastables to a resonant level by electron collision, the metastable number density for the stationary state will decrease, becoming comparable to that of electrons

TABLE II. Results of fitting of the experimental data downstream with the analytic expression for the electron number density.

p (mTorr)	$\langle T_e \rangle$ (eV)	n_0 (10^9 cm^{-3})	n_1 (10^{10} cm^{-3})	z_0 (cm)	k_2[a] (10^{-8} cm^3/s)	k_3 (10^{-12} cm^6/s)	n^* (10^{12} cm^{-3})
0.5	11.24	2.10	0.87	3.86	2.07	2.25	4.63
2.0	5.67	5.90	1.08	2.45	0.30	0.04	3.33

[a]Reference [12], p. 80.

or even one order of magnitude lower than that [15]. More reliable numerical values for n^* and k_3 can be obtained by solving the system of coupled balance equations, having n_e and n^* as variables.

V. SUMMARY AND CONCLUSIONS

Our experimental results prove that a 3D current-free DL can appear in an inductively coupled plasma in a uniform magnetic field. The DL forms inside the source chamber when the collector is electrically floating and close to the entrance of the main chamber when the collector is biased. However, in this latter case, the DL is not a current-free one anymore. Moreover, our results prove that DL's also form at pressures above 1 mTorr, although they become weaker as the pressure increases.

We showed that the obtained DL is the result of a self-organization process taking place inside the plasma column; i.e., it appears as a result of the intrinsic dynamics of the plasma particles, and not as a consequence of an external constraint. The DL is self-assembling during the plasma breakdown and remains in a steady state after that. It acts as an internally built boundary between two plasma regions with different properties: one with high electron temperature and small electron number density (upstream) and one with high electron number density and small electron temperature (downstream). Once formed, the DL plays the role of an internal current source, accelerating electrons downstream.

The proposed physical scenario for the emergence of the current-free DL is based on the quantum processes of excitation and ionization and on the collective interaction between electrons and positive ions, which form two adjacent and opposite space charges inside the plasma source.

In our experiments the electron number density monotonically increases downstream, at least in the probing range. This result is in contradiction with that obtained earlier in the study of potential formations in helicon discharges [5,18], but is similar to other studies on the same type of discharges [19–21]. However, if in [20,21] the downstream electron number density profile was explained as being a consequence of electron pressure balance, in our case the product $n_e T_{e,eV}$ is not constant downstream, but an increasing function of the axial position z. We explained this "excess" of electron pressure downstream by considering the neutral metastable ionization. The obtained analytical model, although the result of some oversimplifications, allows a first evaluation of the metastable number density and of the three-body recombination reaction rate.

APPENDIX A: CURRENT DENSITY INSIDE THE DL

The current density j can be expressed as a function of the potential drop on the DL with the help of Ohm's law:

$$j = \sigma E = \sigma \frac{\Delta V_{DL}}{\Delta z_{DL}}, \tag{A1}$$

where E is the electric field inside the DL.

To determine the value of j, an expression for plasma rf conductivity σ is needed. This can be written as ([12], p. 688)

$$\sigma = \sigma_{dc} \frac{\dfrac{\nu_{en}}{\nu_{eff}}}{1 + \left(\dfrac{\omega_{eff}}{\nu_{eff}}\right)^2}, \tag{A2}$$

ν_{en} being the electron-neutral collision frequency, while ν_{eff} is the effective value of the same quantity; ω_{eff} is the effective rf driving radian frequency and

$$\sigma_{dc} = \frac{e^2 n_e}{m \nu_{en}} \tag{A3}$$

is the dc or low-frequency plasma conductivity. In Eq. (A3), e is the electron charge, m its mass, and n_e its number density.

At pressures below 2 mTorr, $\omega_{eff} = \omega$, where $\omega = 85.20 \times 10^6$ rad/s is the rf driving radian frequency. Also, for electron temperatures above 7 eV (situation valid for both pressures in our experiments), $\nu_{eff} = \nu_{en}$ (see [12], p. 688). Under these circumstances, Eq. (A2) has the form

$$\sigma = \frac{\sigma_{dc}}{1 + \left(\dfrac{\omega}{\nu_{en}}\right)^2}. \tag{A4}$$

The numerical values for plasma conductivity can now be calculated, allowing numerical estimation of the current density passing through the DL. Hence, introducing Eq. (A3) in Eq. (A4) and the result in Eq. (A1), we get

$$j = \frac{\dfrac{e^2 n_e}{m \nu_{en}}}{1 + \left(\dfrac{\omega}{\nu_{en}}\right)^2} \frac{\Delta V_{DL}}{\Delta z_{DL}}. \tag{A5}$$

APPENDIX B: SOLUTION OF THE DIFFUSION EQUATION

Before solving Eq. (4), we can find the value of the electron concentration "far away" downstream, where it will be uniform ($n_e = n_0 = \text{const}$ or, equivalently, the loss and gain processes will compensate each other):

$$n_0 = \sqrt{\frac{\psi}{\xi}}. \tag{B1}$$

Multiplying both sides of Eq. (4) by the axial gradient of the electron number density $\partial n_e/\partial z$ and integrating, we obtain

$$\left(\frac{\partial n_e}{\partial z}\right)^2 = \frac{1}{2}\xi n_e^4 - \psi n_e^2 + C_1. \tag{B2}$$

The integration constant C_1 can be easily found by using Eq. (B1). In these conditions, after rearranging the terms, extracting the square root, and taking into account that the electron number density is an increasing function of the axial distance z and also that $n_e \leqslant n_0$, Eq. (B2) becomes

$$\frac{\partial n_e}{\partial z} = \sqrt{\frac{\xi}{2}}(n_0^2 - n_e^2). \tag{B3}$$

Separating the variables, this equation can be integrated and the result is

$$n_e(z) = n_0 \tanh\left[n_0\sqrt{\frac{\xi}{2}}(z - z_0)\right], \tag{B4}$$

z_0 being an integration constant (i.e., the inflection point of the hyperbolic tangent function).

From Eq. (B4) it follows that in the inflection point $z = z_0$, $n_e(z_0) = 0$; hence, n_e is defined only for $z > z_0$. However, the experimental data show that the electron number density is positive for a relatively large interval around the inflection point. This means that the entire graph of the solution (B4) is shifted upwards on a "distance" equal to the electron number density in the inflection point. Denoting this density by n_1, Eq. (B4) becomes

$$n_e(z) = n_1 + n_0 \tanh\left[n_0\sqrt{\frac{\xi}{2}}(z - z_0)\right]. \tag{B5}$$

Since, in both pressure ranges, the electron number density downstream increases from a given value n_{e1} to another one n_{e2}, each dependent on pressure, the relationships between $n_{0,1}$ and $n_{e1,2}$ are

$$n_0 = \frac{1}{2}(n_{e2} - n_{e1}),$$

$$n_1 = \frac{1}{2}(n_{e2} + n_{e1}). \tag{B6}$$

With the constants given by Eq. (B6), Eq. (B5) describes the spatial variation of the electron number density downstream.

[1] I. Langmuir, Phys. Rev. **33**, 954 (1929).
[2] H. Alfvén, Tellus **10**, 104 (1958).
[3] M. A. Raadu, Phys. Rep. **178**, 25 (1989).
[4] Sendai Plasma Forum, *Double Layers–Potential Formation and Related Nonlinear Phenomena in Plasmas*, edited by Sendai "Plasma Forum" (World Scientific, Singapore, 1997).
[5] C. Charles and R. Boswell, Appl. Phys. Lett. **82**, 1356 (2003).
[6] X. Sun, A. M. Keesee, C. Biloin, E. E. Scime, A. Meige, C. Charles, and R. W. Boswell, Phys. Rev. Lett. **95**, 025004 (2005) and references therein.
[7] F. F. Chen (unpublished).
[8] F. F. Chen (unpublished).
[9] B. L. Stansfield, in M. Sugawara, *Plasma Etching—Fundamentals and Applications* (Oxford University Press, New York, 1998), pp. 101–179.
[10] M. Sanduloviciu, E. Lozneanu, and S. Popescu, Chaos, Solitons Fractals **17**, 183 (2003).
[11] W. L. Theisen, R. T. Carpenter, and R. L. Merlino, Phys. Plasmas **1**, 1345 (1994).
[12] M. A. Lieberman and A. J. Lichtenberg, *Principles of Plasma Discharges and Materials Processing*, 2nd ed. (Wiley-Interscience, Hoboken, NJ, 2005).
[13] T. Makabe, N. Nakano, and Y. Yamaguchi, Phys. Rev. A **45**, 2520 (1992).
[14] D. P. Lymberopoulos and D. J. Economou, J. Res. Natl. Inst. Stand. Technol. **100**, 473 (1995).
[15] G. A. Hebner, J. Appl. Phys. **80**, 2624 (1996).
[16] C. Diplasu, A. Surmeian, and H. Fujita, J. Optoelectron. Adv. Mater. **7**, 2397 (2005).
[17] J. Ma and Y. K. Pu, Phys. Plasmas **10**, 4118 (2003).
[18] C. Charles and R. W. Boswell, Phys. Plasmas **11**, 1706 (2004).
[19] X. M. Guo, J. Scharer, Y. Mouzouris, and L. Louis, Phys. Plasmas **6**, 3400 (1999).
[20] I. D. Sudit and F. F. Chen, Plasma Sources Sci. Technol. **5**, 43 (1996).
[21] F. F. Chen, I. D. Sudit, and M. Light, Plasma Sources Sci. Technol. **5**, 173 (1996).